Up-regulated IL-17 and Tnf signaling in bone marrow cells of young male osteogenesis imperfecta mice

Chenyi Shao[1,*], Yi Liu[1,*], Jiaci Li[2], Ziyun Liu[1], Yuxia Zhao[1], Yaqing Jing[1], Zhe Lv[1], Ting Fu[1], Zihan Wang[1] and Guang Li[1]

[1] Tianjin Medical University, Tianjin, China
[2] Tianjin Pediatric Research Institute, Tianjin Children's Hospital, Tianjin, Longyan Road, Beichen District, Tianjin, China
[*] These authors contributed equally to this work.

ABSTRACT

Osteogenesis imperfecta (OI) is a congenital bone dysplasia mainly caused by either defective production or assembly of type I collagen. The skeletal phenotypes especially fractures are often seen in OI adolescents. Studies have found that an increased number of osteoclasts and excessive bone resorption existed in collagen-related OI, which has not been well understood. Emerging evidence has suggested that inflammation may be associated with OI. We speculated that the bone marrow (BM) niche had similar inflammatory changes and performed RNA-sequencing (RNA-seq) in BM cells derived from young male mice to analyze the related differentially expressed genes (DEGs) and pathways. Data showed that there were 117 shared DEGs ($Q \leq 0.05$, $|\log_2 FC| \geq 1$) in BM cells isolated from two types of OI murine models that respectively simulate different OI types. Gene Ontology (GO) ($Q \leq 0.05$) analysis, Kyoto Encyclopedia of Genes and Genomes (KEGG) ($Q \leq 0.05$) analysis and real-time PCR validation indicated the dysregulated biology process of cellular response to interferon (Ifn) together with upregulated IL-17 signaling, tumor necrosis factor (Tnf) signaling and osteoclast differentiation in OI BM niche. Either defective collagen production or abnormal collagen assembly shared similar alterations in gene profiles and pathways involving inflammation and osteoclast activation. Data presented here not only contributed to understanding of the mechanism of the enhanced bone absorption in the bones of OI, but also provided more evidence to develop potential anti-inflammation therapies.

Subjects Biochemistry, Bioinformatics, Cell Biology, Molecular Biology
Keywords Osteogenesis imperfecta, Bone resorption, RNA sequencing, Bone marrow, Inflammation

HIGHLIGHT

1. There were 117 shared differentially expressed genes in bone marrow (BM) cells isolated from two types of OI young male murine models.
2. The upregulated IL-17 signaling, Tnf signaling and osteoclast differentiation were significantly enriched in OI BM cells.

Submitted 24 May 2022
Accepted 8 August 2022
Published 23 August 2022

Corresponding author
Guang Li, lig@tmu.edu.cn

Academic editor
Eva Mezey

Additional Information and Declarations can be found on page 12

DOI **10.7717/peerj.13963**

How to cite this article Shao C, Liu Y, Li J, Liu Z, Zhao Y, Jing Y, Lv Z, Fu T, Wang Z, Li G. 2022. Up-regulated IL-17 and Tnf signaling in bone marrow cells of young male osteogenesis imperfecta mice. **PeerJ 10:e13963 DOI 10.7717/peerj.13963**

3. These dysregulated DEGs and pathways in BM cells might be associated with the excessive bone resorption of the OI mice.

INTRODUCTION

Osteogenesis imperfecta (OI) is a congenital disorder characterized by bone fragility (*Forlino et al., 2011*). The patients generally suffer from recurrent bone fractures and deformities. Up to 21 genes have been associated with OI, but most of the total cases are caused by heterozygous mutation in either of the genes coding for the type I collagen alpha chains, *COL1A1* or *COL1A2* (*Forlino et al., 2011*). The pathogenic variants of the two genes often cause either insufficient synthesis or abnormal structure of skeletal collagen, which is correlated with mild OI type I and more severe type II–IV respectively (*Saito & Marumo, 2015*; *Nijhuis et al., 2019*).

Multiple reports have highlighted the impaired bone formation and excessive bone absorption in defective collagen-related OI (*Takeyari et al., 2021*; *Iwamoto, Takeda & Ichimura, 2002*), which are the main targets in OI treatments. Type I collagen fibrils are produced by bone-forming osteoblasts, making the dysfunctional osteoblasts and their weakened mineralization the main focus of OI etiological research. Conversely, the mechanism of enhanced bone destruction in OI bones has not been well understood, although anti-resorptive drugs have been widely applied in clinical interventions.

Some recent studies have indicated the contribution of inflammation and inflammatory factors in OI bone phenotype. Increased transformation growth factor-beta (TGF β) and excessive TGF signaling have been regarded as a promising target to enhance bone formation in some OI models and patients (*Grafe et al., 2014*; *Marom, Rabenhorst & Morello, 2020*). Also, the elevated serum level of interferon (IFN) and tumor necrosis factor (TNFα) have been found in patients and mouse models separately, suggesting the chronic inflammation state in OI (*Zhytnik et al., 2020*). Inflammation has been closely linked to bone biochemical changes and bone loss in rheumatoid arthritis (RA) and osteoporosis (*Weyand & Goronzy, 2021*; *Tilg et al., 2008*). The progenitor cells of osteoblasts and osteoclasts derived from hematopoietic stem cell (HSC) lineage are both situated in the same bone marrow (BM) niche (*Ono & Nakashima, 2018*). The inflammatory alterations of the BM niche that have not been well explored may directly or indirectly act on the bone manifestations of OI.

In the process of bone marrow development, the transformation of red bone marrow to yellow bone marrow is most obvious in infancy and childhood (*Berg, 2021*). Compared with the old bone marrow, the level of ROS in the young bone marrow is lower, and the cells are less affected by aging, which can better reflect the initial bone marrow state under genetic defects (*Yao et al., 2021*). Also, the skeletal symptoms of OI are most obvious in childhood and can be relieved in adulthood (*Paterson, McAllion & Stellman, 1984*). Studying the bone marrow of young mice will help to understand the cause and process of OI. Here, we performed RNA-sequencing (RNA-seq) and differential gene expression analyses in femoral BM cells isolated from young mice of two types of OI mouse models and wild-type mice to explore the changes in the BM niche. Both the $Col1a1^{+/-365}$ mice and heterozygous oim mice (*Col1a2*$^{oim/+}$) display osteogenesis deficiency accompanied by an increased number of osteoclasts. The differentially expressed genes (DEGs) shared by the two OI models were involved in IL-17 signaling pathway, Tnf signaling pathway and osteoclast differentiation. The DEGs related to the three pathways were all upregulated in OI BM cells when compared with normal cells, suggesting the activation of these signalings. These dysregulated genes and pathways in mutant BM cells are likely to play an important role in the pathological changes of OI bones.

MATERIALS AND METHODS

OI mice model

Adult wild-type (wt) C57BL/6 mice were purchased from the Laboratory Animal Center of the Academy of Military Medical Science (China). The B6C3Fe a/a-*Col1a2*^{oim}/J mice (#001815) were bought from the Jackson Laboratory (Bar Harbor, ME, USA) and maintained on a congenic C57BL/6 background. The *Col1a2*$^{oim/+}$ mice were heterozygotes carrying a single mutant *Col1a2* allele and performed a mild form of OI. The *Col1a1*$^{+/-365}$ mice with a *Col1a1* gene knock-down can simulate OI type I. Heterozygous mice were bred by crossing heterozygous individuals and genotyped as previously described (*Chipman et al., 1993*; *Liu et al., 2019*). All mice were housed in specific pathogen-free conditions and sacrificed by CO_2 in 4 weeks old to sample. Mice were fed with full-price diet and autoclaved water. The number of mice per cage did not exceed five. All experiments were performed following the approval of Animal Care and Use Committee of Tianjin Medical University (TMUaMEC 2017012). Only male mice were used in the present study.

Cell isolation

The femurs of 4-weeks and 12-weeks old male mice were harvested and the bone marrow (BM) cells were flushed out with a syringe. The wt and OI modeled mice-derived BM cells were marked as BM^{wt}, $BM^{oim/+}$ and $BM^{+/-365}$ respectively.

RNA extraction and RNA sequencing (RNA-seq)

Total RNA of freshly isolated BM cells was extracted using Trizol reagents (Invitrogen, Waltham, MA, USA). Each type of cells isolated from one mouse was seen as one sample and each group contained three samples. RNA samples (n = 3/genotype from young animals) with RNA integrity number ≥ 7.0 and 28S/18S ratios ≥ 1.5 were sequenced. Another 18 RNA samples (n = 6/genotype) were used in quantitative PCR verification.

A total of 18 cDNA libraries were constructed and separately sequenced by Beijing Genomics Institute (BGI, Beijing, China) using the BGISEQ-500 platform. RNASeqPower Software were used to calculated the statistical power of this experimental design. Sequence data (~75 million reads) were checked for sequencing quantity by FASTQC. Reads with low quality (unknown nucleotides > 10%, or Q20 < 20%), adapter contamination and high N content of unknown bases (N > 5%) were excluded to gain clean reads. The clean reads were then mapped to the mouse reference genome (Mus_musculus, NCBI, GCF_000001635.26_GRCm38.p6) and analyzed by HISAT2 software. Read counts were normalized to TPM (transcripts per kilobase of exon model per million mapped reads).

Table 1 Sequences of primers used for RT-PCR.

Gene	Forward (5′-3′)	Reverse (5′-3′)	Product length (bp)
Lif	TCAACTGGCACAGCTCAATGGC	GGAAGTCTGTCATGTTAGGCGC	119
Jun	CCTTCTACGACGATGCCCTC	GGTTCAAGGTCATGCTCTGTTT	102
Fosb	TTTTCCCGGAGACTACGACTC	GTGATTGCGGTGACCGTTG	174
Stat1	TCACAGTGGTTCGAGCTTCAG	GCAAACGAGACATCATAGGCA	155
Cxcl10	CCAAGTGCTGCCGTCATTTTC	GGCTCGCAGGGATGATTTCAA	157
Ccl2	TTAAAAACCTGGATCGGAACCAA	GCATTAGCTTCAGATTTACGGGT	121
Ifng	ATGAACGCTACACACTGCATC	CCATCCTTTTGCCAGTTCCTC	182
Ifit1	GCCTATCGCCAAGATTTAGATGA	TTCTGGATTTAACCGGACAGC	75
Irf7	GAGACTGGCTATTGGGGGAG	GACCGAAATGCTTCCAGGG	102
Gapdh	CATCACTGCCACCCAGAAGACTG	ATGCCAGTGAGCTTCCCGTTCAG	153

Note:
Lif, leukemia inhibitory factor; Jun, jun proto-oncogene; Fosb, FBJ osteosarcoma oncogene B; Stat1, signal transducer and activator of transcription 1; Cxcl10, chemokine (C-X-C motif) ligand 10; Ccl2, chemokine (C-C motif) ligand 2; Ifng, interferon gamma; Ifit1, interferon-induced protein with tetratricopeptide repeats 1; Irf7, interferon regulatory factor 7; Gapdh, glyceraldehyde-3-phosphate dehydrogenase.

Q-value was obtained by false discovery rate (FDR) correction of the *P*-value. Differentially expressed genes (DEGs) ($Q \leq 0.05$, $|\log_2 FC| \geq 1$) were analyzed by DEseq2 software. Gene Ontology (GO) ($Q \leq 0.05$) and Kyoto Encyclopedia of Genes and Genomes (KEGG) ($Q \leq 0.05$) analyses were performed in DEGs shared by the two OI models derived BM cells using BGI Dr. Tom multi-omics data mining system. Gene Set Enrichment Analysis (GSEA) based on the KEGG database was also performed using BGI Dr. Tom and results with $P \leq 0.05$ and $Q \leq 0.25$ were considered statistically significant.

Quantitative real-time PCR (RT-PCR)

The RNA samples from both young and adult mice were reverse transcribed to cDNA using GoScript reverse transcriptase (Promega, Madison, WI, USA) according to the manufacturer's protocol. RT-PCR analysis was performed using the AceQ RT-PCR SYBR Green Master Mix kit (Vazyme, Nanjing, China). The cycling program referenced our previous report (*Liu et al., 2020*). All samples were evaluated in triplicate and normalized to mouse *glyceraldehyde-3-phosphate dehydrogenase* (*Gapdh*). All the primers were synthesized from Sangon Biotech Co., Ltd. (China), and the sequences were listed in Table 1.

Statistical analysis

Statistical analysis was conducted using SPSS version 17.0 software (IBM SPSS Statistics, Chicago, IL, USA). All data were presented as mean ± standard deviation (SD).
Two groups were generally compared by unpaired. The D'Agostino-Pearson omnibus normality test was used to test the normal distribution of data. If the data conformed to the normal distribution ($P > 0.1$), the unpaired t-test was used. In the unpaired t-test, the F-test was used to analyze the homogeneity of variance for pairwise comparison. If the variance was homogenous ($P > 0.05$), the unpaired t-test was performed. If variances were not homogeneous ($P < 0.05$), Welch's correction was used to correct them. If the data were not

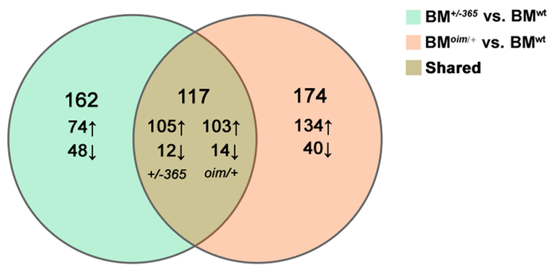

Figure 1 The results of RNA-seq of bone marrow (BM) cells. The Venn diagram of differentially expressed genes (DEGs) in BM cells isolated from 4-weeks old wt mice, heterozygous *Col1a1*$^{+/-365}$ and *Col1a2*$^{oim/+}$ mice ($Q \leq 0.05$, $|\log_2 FC| \geq 1$). There were 117 DEGs shared by the two types of OI mice.
Full-size DOI: 10.7717/peerj.13963/fig-1

subject to a normal distribution, the Mann-Whitney test was used. $P < 0.05$ was considered statistically significant.

RESULTS

Differential gene expression analysis

RNA-seq was performed in BM cells of the three genotypes of mice. The statistical power (depth = 100, cv = 0.1, effect = 2, $\alpha = 0.05$, power = 0.9) of this experimental design, calculated in RNASeqPower was 0.0875. Compared with BM^{wt}, a total of 279 DEGs were identified in BM$^{+/-365}$ and 219 of which were upregulated and 60 were downregulated (Fig. 1). A total of 291 DEGs were differentially expressed in BM$^{oim/+}$ when compared with BM^{wt}, 237 of which were upregulated and 54 were downregulated (Fig. 1). There were 117 DEGs shared by the two types of OI mice (Fig. 1). A total of 102 of the common DEGs were concordantly upregulated and 12 were concordantly downregulated, suggesting their consistency of alteration (Data not shown).

The top 20 upregulated shared DEGs in BM$^{+/-365}$ or BM$^{oim/+}$ were listed in Tables 2 and 3 respectively. A total of 17 of them were the same genes that contained several Ifn signaling-related genes (*e.g.*, *Lfit1*, *Lfit3*, *Lfi44* and *Irf7*) (Tables 2 and 3). Notably, the transcription of *Coch*, most abundantly expressed in the inner ear, was obviously increased in the two types of BM cells (Tables 2 and 3). The abnormal *Coch* expression might be associated with OI hearing loss.

Gene Ontology biology process analysis

Gene Ontology (GE) biology process analysis indicated the enrichment of multiple immune-related genes in such as cellular response to interferon-beta (Ifnβ), immune system process, and immune response, and cellular response to interferon-alpha (Ifnα) in defective BM cells (Fig. 2A). We tested the level of *Lfit1* and *Irf7*, and data showed that both of the two genes were significantly upregulated in mutant BM cells (Figs. 2B and 2C), suggesting the activated Ifn signaling in OI BM.

KEGG pathway enrichment and GSEA analysis

The significantly enriched pathways by KEGG analysis of the 117 shared DEGs included the IL-17 signaling pathway, Tnf signaling pathway and osteoclast differentiation in OI

Table 2 The top 20 upregulated shared DEGs in $BM^{+/-365}$ when compared with BM^{wt}.

Gene	Description	Log2 (Fold chang)	Q-value
Fgf23	fibroblast growth factor 23	5.83	0.0002360794650486
Ptgds	prostaglandin D2 synthase (brain)	5.54	0.0021177353272204
Oas1g	2'–5' oligoadenylate synthetase 1G	4.9	0.0009431000835065
Apol9b	apolipoprotein L 9b	4.6	0.0002133173066225
Ifit1	interferon-induced protein with tetratricopeptide repeats 1	4.28	0.0003668837536278
Ifit3	interferon-induced protein with tetratricopeptide repeats 1	4.25	0.0015924514011703
Ifi44	interferon-induced protein 44	4.17	0.003021888072243
Coch	coagulation factor C homology/cochlin	4.11	0.0260410468387774
Isg15	ISG15 ubiquitin-like modifier	3.98	0.0000106275044397477
Ifit3b	interferon-induced protein with tetratricopeptide repeats 3b	3.91	0.001908267305679
Rsad2	radical S-adenosyl methionine domain containing 2	3.38	1.62699675914253e−13
Usp18	ubiquitin specific peptidase 18	3.24	0.0010491995647924
Oas1a	2'–5' oligoadenylate synthetase 1A	3.05	0.0016396718614034
Oasl2	2'–5' oligoadenylate synthetase 2	3	0.0031321485213441
Gbp6	guanylate binding protein 6	3	0.0010429030626467
Irf7	interferon regulatory factor 7	2.98	0.002419157920696
Cfb	complement factor B	2.97	0.0133696378926878
Gbp10	guanylate-binding protein 10	2.97	0.0013662770771023
Zbp1	Z-DNA binding protein 1	2.9	0.0088547659475085
Rtp4	receptor transporter protein 4	2.85	0.0013424962435546

BM cells (Fig. 3A). There were 11 enriched DEGs involved in the aforementioned pathways (Table 4). GSEA analysis demonstrated that all of the three pathways were markedly upregulated in OI-derived BM cells (Figs. 3B–3D). Besides, the sequencing data demonstrated that both *I117a* and *Tnf* increased more than two-fold in $BM^{oim/+}$ (Table 5). The *Tnf* expression also got significantly elevated in *Col1a1*$^{+/365}$ mice-derived BM cells (Table 5). In addition, the mRNA level of *Rankl* (*Tnfsf11*) rose in defective BM cells (Table 5). It has been reported that upregulated IL-17 and Tnf signalings contribute to the excessive bone resorption in multiple inflammatory bone loss diseases (*Tsukasaki & Takayanagi, 2019*; *Weitzmann, 2017*), suggesting the potential role of overactivated IL-17 and Tnf pathways in an increased number of osteoclasts under the OI background.

The changes of DEGs in BM cells isolated from OI modeled mice

The heatmap as shown in Fig. 4A displayed the differential expression of the 11 DEGs mentioned above. Many of them at least participate in two of the IL-17 signaling pathway, Tnf signaling pathway, and osteoclast differentiation, suggesting their complex crosstalk. RT-PCR validation indicated that *Ccl2* (Fig. 4B), *Jun* (Fig. 4C) *Cxcl10* (Fig. 4D), *Lif* (Fig. 4E) and *Stat1* (Fig. 4F) were apparently upregulated in mutant BM cells, which was consistent with the sequencing data. And *Fosb* (Fig. 4G) and *Ifng* (Fig. 4H) expression also showed an increasing trend in OI mice-derived BM cells. These results preliminarily identified the dysregulated DEGs, which might play important roles in OI bone erosion alterations.

Table 3 The top 20 upregulated shared DEGs in BM$^{oim/+}$ when compared with BM^{wt}.

Gene	Description	Log2 (Fold chang)	Q-value
Ptgds	prostaglandin D2 synthase (brain)	7.5	6.17204589560265e−9
Coch	coagulation factor C homology/cochlin	6.02	2.94335300566472e−8
Oas1g	2'–5' oligoadenylate synthetase 1G	5.18	9.681071247414061e−14
Fgf23	fibroblast growth factor 23	4.99	0.000606927029448
Ifi44	interferon-induced protein 44	4.46	1.23002041345624e−21
Ifit3	interferon-induced protein with tetratricopeptide repeats 3	4.44	1.08339825790861e−9
Ifit1	interferon-induced protein with tetratricopeptide repeats 1	4.22	5.155872680064089e−11
Ifit3b	interferon-induced protein with tetratricopeptide repeats 3b	4.2	9.503797111990189e−11
Gbp6	guanylate binding protein 6	3.63	1.1575697141787101e−74
Apol9b	apolipoprotein L 9b	3.52	0.0012727812836212
Cfb	complement factor B	3.47	9.1080396056311e−39
Isg15	ISG15 ubiquitin-like modifier	3.37	7.51494012126258e−18
Tgtp1	T cell specific GTPase 1	3.36	1.28520549551154e−10
Oasl2	2'–5' oligoadenylate synthetase 2	3.19	1.83115647109809e−26
Gbp10	guanylate-binding protein 10	3.19	3.41807441735383e−13
Oas1a	2'–5' oligoadenylate synthetase 1A	3.15	3.8026707877775104e−15
Usp18	ubiquitin specific peptidase 18	3.14	1.29677254526075e−14
Iigp1	interferon inducible GTPase 1	3.14	0.000013763932948896
Irf7	interferon regulatory factor 7	3.12	6.5309598268511e−36
Ly6i	lymphocyte antigen 6 complex, locus I	3.1	3.91587391622785e−21

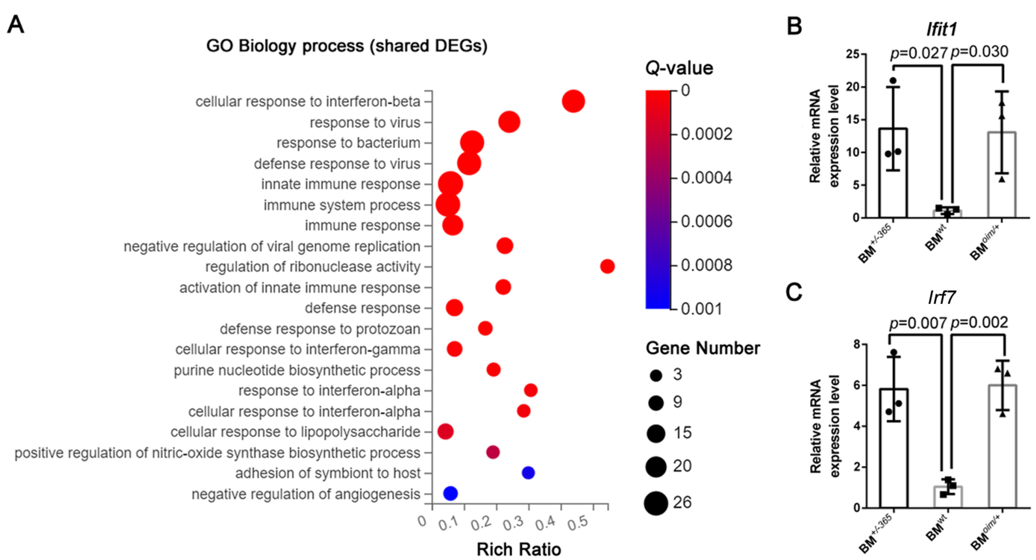

Figure 2 The results of GO Biology process analysis of the shared DEGs. (A) Top 20 GO Biology process analysis enrichments of the shared 117 DEGs of BM$^{+/-365}$ and BM$^{oim/+}$ ($Q \leq 0.05$). Multiple immune-related DEGs were enriched in cellular response to interferon. The size of the spot represents the number of differential genes, the color represents the Q value; (B, C) Real-time PCR identified the expression levels of *Lfit1* (B) and *Irf7* (C) in BM cells isolated from 4-weeks old wt, heterozygous *Col1a1*$^{+/-365}$ and *Col1a2*$^{oim/+}$ mice (n = 3, P < 0.05). The result indicated that both of the two genes were significantly up-regulated in BM$^{+/-365}$ and BM$^{oim/+}$. Data in the quantitative plots are presented as mean ± SD using upaired t-test. Full-size DOI: 10.7717/peerj.13963/fig-2

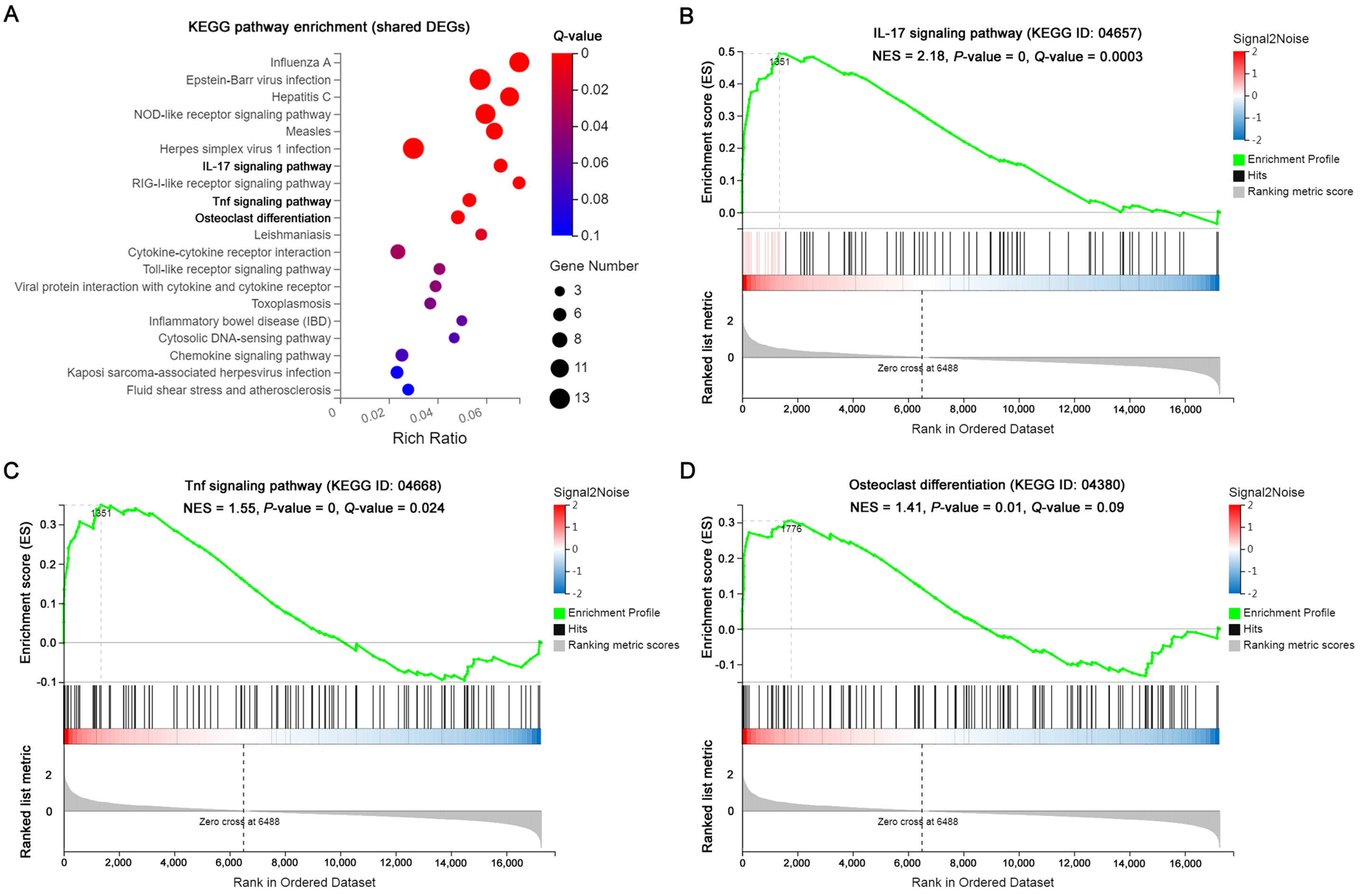

Figure 3 The results of KEGG pathway enrichment and GSEA analysis of the shared DEGs. (A) Top 20 KEGG analysis enrichments of the shared 117 DEGs of BM$^{+/-365}$ and BM$^{oim/+}$. The significantly enriched pathways of the shared DEGs included the IL-17 signaling pathway, Tnf signaling pathway and osteoclast differentiation in OI BM cells ($Q \leq 0.05$). The size of the spot represents the number of differential genes, the color represents the Q value. (B–D) The GSEA analysis of the aforementioned three pathways ($P \leq 0.05$ and $Q \leq 0.25$). The results demonstrated that all of the three pathways were markedly upregulated in OI-derived BM cells. Full-size DOI: 10.7717/peerj.13963/fig-3

Besides, the expression of these genes in adult mice was also detected by RT-PCR. Data showed that *Tnfα* (Fig. S1C), *Lif* (Fig. S1D), and *Ccl2* (Fig. S1E) were still elevated in mutant BM cells when compared to the normal cells, although there were no differences in the expression of *Ifit1* (Fig. S1A), *Jun* (Fig. 1F), *Stat1* (Fig. S1G) and *Cxcl10* (Fig. S1H). The obviously increased level of *Irf7* (Fig. S1B) and *Ifng* (Fig. S1I) in BM$^{oim/+}$ instead of BM$^{+/-365}$ could be observed in RT-PCR assay. The IL-17 signaling pathway, Tnf signaling pathway and osteoclast differentiation under OI background remained up-regulated until adulthood.

DISCUSSION

OI is mainly caused by the defective production or assembly of type I collagen, making bone tissue severely affected (*Forlino et al., 2011*; *Hoyer-Kuhn, Netzer & Semler, 2015*). OI patients with *COL1A1* or *COL1A2* mutations can be classified into OI type I-IV

Table 4 **The shared DEGs involved in 'IL-17 signaling pathway', 'Tnf signaling pathway' and 'osteoclast differentiation' of $BM^{+/-365}$ and $BM^{oim/+}$ when compared with BM^{wt}.**

Gene	Description	Log2 (Fold chang)		Q-value	
		$BM^{+/-365}$	$BM^{oim/+}$	$BM^{+/-365}$	$BM^{oim/+}$
Ccl2	chemokine (C-C motif) ligand 2	2.73	2.92	5.23025917899991e−16	0.00000124536325640583
Gm5431	predicted gene, 45935	1.11	1.47	0.0421644826331762	4.85491962362027e−9
Cxcl10	chemokine (C-X-C motif) ligand 10	2.09	1.57	0.0009539010036805	0.0028754859114639
Lif	leukemia inhibitory factor	1.46	1.70	0.0098724762681209	0.0024271897572989
Ifng	interferon gamma	1.71	2.15	0.0002510762900628	2.01552889198521e−7
Fosb	FBJ osteosarcoma oncogene B	2.40	2.23	0.00000208273094362867	0.0008131293868126
Stat1	signal transducer and activator of transcription 1	1.27	1.47	0.0000710335367185181	4.59990999943035e−23
Jund	jun D proto-oncogene	1.00	1.04	0.0015850803802578	2.41298702546188e−14
Jun	jun proto-oncogene	1.86	1.66	4.2489456147999705e−20	1.75119110664004e−52
Lfi47	interferon-induced protein 47	1.62	1.75	0.0247317221652343	5.43681272346479e−24
Fcgr1	Fc receptor, IgG, high affinity I	2.13	2.63	0.0033203206673691	1.34407141389434e−33

Table 5 **Some key genes that were not shared DEGs involved in 'IL-17 signaling pathway', 'Tnf signaling pathway' and 'osteoclast differentiation' of $BM^{+/-365}$ and $BM^{oim/+}$ when compared with BM^{wt}.**

Gene	Description	Log2 (Fold Chang)		Q-value	
		$BM^{+/-365}$	$BM^{oim/+}$	$BM^{+/-365}$	$BM^{oim/+}$
Tnf	tumor necrosis factor	0.77	1.21	0.0110345421756999	2.8259877145669397e−13
Il17a	interleukin 17A	2.98	4.62	0.529929360546415	0.0204958961911906
Tnfrsf11a	tumor necrosis factor receptor superfamily, member 11a, NFKB activator/Rank	−0.004	0.20	0.996564355301463	0.791864645628747
Tnfsf11	tumor necrosis factor (ligand) superfamily, member 11/Rankl	1.09	0.95	0.587237549231164	0.486382634245118

phenotypes (*Forlino et al., 2011*). OI type I due to decreased synthesis of collagen fibrils shows the mildest phenotype, while structurally aberrant type I collagen can give rise to much more severe type II–IV. Despite the subtypes and caused pathogenic variants, high bone turnover represented by hypercellular osteocytes but insufficient mineralization together with enhanced bone absorption generally exist in collagen defect-related OI (*Liu et al., 2019*; *Lopez Franco et al., 2005*; *McBride, Shapiro & Dunn, 1998*; *Saban et al., 1996*). Many studies have focused on the mechanism underlying the unit bone formation insufficiency, while excessive bone erosion has not been extensively explored.

Bone resorption is mainly mediated by osteoclasts that originate from HSC-derived monocytes (*Boyle, Simonet & Lacey, 2003*). The BM monocytes can differentiate into mature multinucleated osteoclasts in the presence of macrophage-colony stimulating factor (M-CSF) and receptor activator of nuclear factor kappa B ligand (RANKL) (*Boyle, Simonet & Lacey, 2003*; *Feng, Guo & Li, 2019*). It has been proved that inflammatory cytokines such as TNFα can act synergistically with RANKL to promote osteoclastotogenesis (*Zhao et al., 2012*). Recently, the inflammatory component in OI pathogenesis has been increasingly attractive. The chronic inflammation state of OI

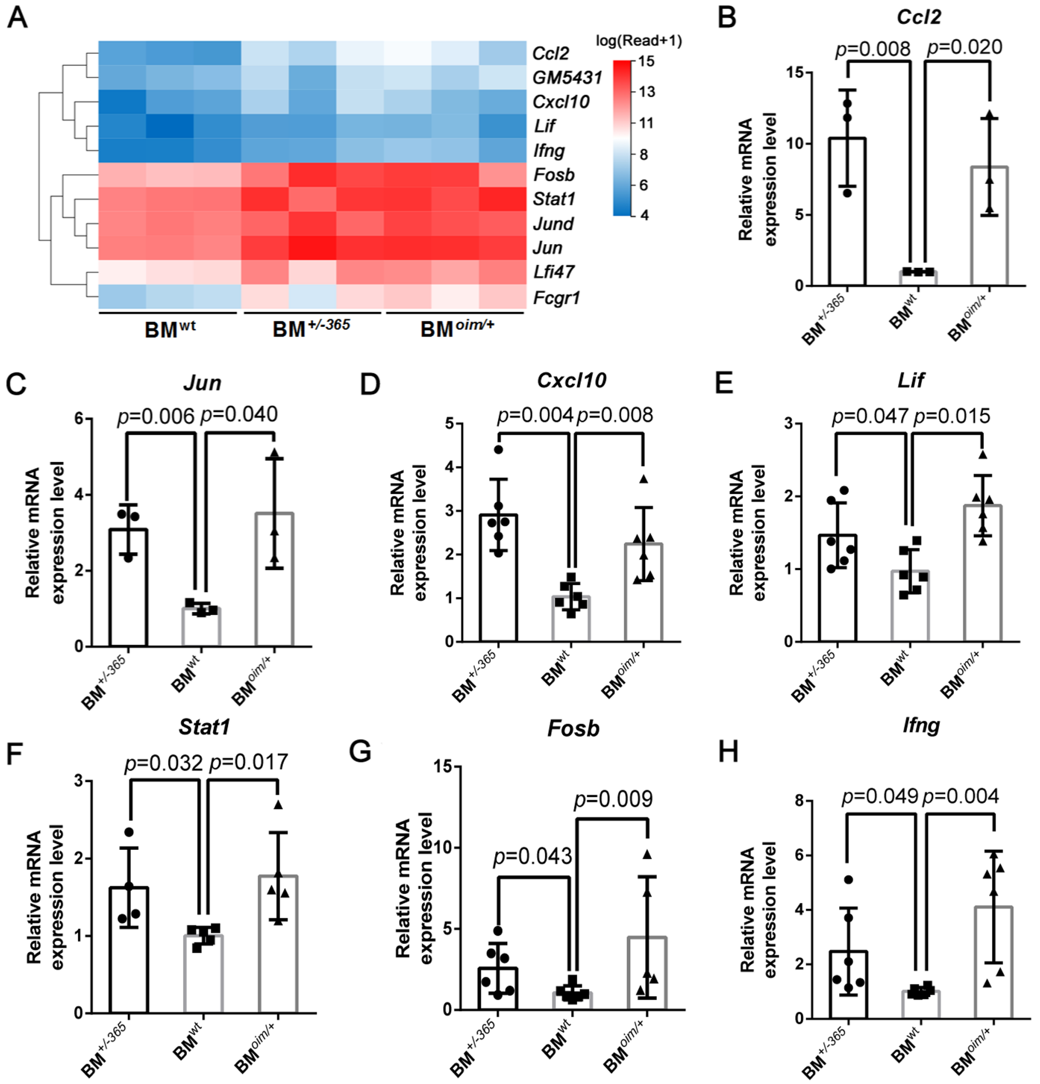

Figure 4 **The expression of the shared DEGs involving IL-17 signaling pathway, Tnf signaling pathway and osteoclast differentiation in BM$^{+/-365}$ and BM$^{oim/+}$ when compared with BM^{wt}.** (A) The heatmap of the 11 DEGs involved in IL-17 signaling pathway, Tnf signaling pathway and osteoclast differentiationof 4-weeks BM cells. (B–G) Real-time PCR tested the expression levels of some DEGs. The result indicated that *Ccl2* (B) and *Jun* (C) were apparently upregulated in mutant BM cells. The obviously increased level of *Cxcl10* (D) in BM$^{+/-365}$ together with *Lif* (E) and *Stat1* (F) in BM$^{oim/+}$ could be observed. *Fosb* (G) and *Ifng* (H) also showed an significantly increased in OI BM cells (n = 3 for B, C, n = 6 for D, E, G, H, n = 4 for F, $P < 0.05$). Data in the quantitative plots are presented as mean ± SD using upaired t-test (B–F, H) and Mann-Whitney test (G). Full-size DOI: 10.7717/peerj.13963/fig-4

murine models and pediatric patients has been suggested by their elevated serum levels of inflammatory cytokines including IFN and TNFα (*Zhytnik et al., 2020*; *Brunetti et al., 2016*). Many clues suggest that the cells and cytokines of the BM niche can regulate the maturation and function of osteoclasts through direct contact and the paracrine effect (*Herrmann & Jakob, 2019*; *Ciucci et al., 2015*). But the inflammatory changes in BM cells are still unclear.

OI is a type of congenital genetic disease, with the most severe symptoms in childhood (*Paterson, McAllion & Stellman, 1984*). Therefore, exploration of the molecular changes of bone marrow cells of OI in early childhood is helpful to understand its pathogenesis.

Here, we performed RNA-seq of whole BM cells isolated from two types of OI models that respectively stimulate abnormal quantity and structure collagen-related OI. Data showed that the BM cells from the two young murine models shared 117 DEGs ($Q \leq 0.05$, $|Log_2FC| \geq 1$) (Fig. 1). A total of 17 of the top 20 upregulated shared DEGs were the same genes, including several Ifn signaling-related genes containing *Lfit1*, *Lfit3*, *Lfi44* and *Irf7* (Tables 2 and 3). Consistent with the findings of Zhytnik's group, GO biology process analysis also enriched multiple DEGs involved in the cellular response to Ifnβ and Ifnα in defective BM cells (Fig. 2), suggesting the activated Ifn signaling in OI BM. Transcription factor STAT1 is a key effector of the IFN pathway (*Michalska et al., 2018*). The upregulated *Stat1* in OI BM cells (Fig. 4F) further revealed the dysregulated Ifn signaling. IFNs are key cytokines for both innate and adaptive immune responses (*Takayanagi et al., 2005*). Some previous studies found that IFN-γ can promote osteoclastogenesis under T-cells activation and enhance the multinucleation of myeloid lineage cells in osteoporosis (*Biros et al., 2022*). Thus the overactivated Ifn signaling might also act on the bone resorption in the OI background.

KEGG and GSEA analysis of the 117 shared DEGs showed that the IL-17 signaling pathway, Tnf signaling pathway and osteoclast differentiation were significantly upregulated in OI BM cells (Fig. 3). A total of 11 enriched DEGs were involved in the three pathways and displayed complex crosstalk (Table 4). *Il17a*, *Tnf* and *Rankl* showed different degrees of upregulation (Table 5), indicating the chronic inflammation and enhanced osteoclastogenesis. RT-PCR assay confirmed the elevated expression of some DEGs in young and adult mice (Fig. 4, Fig. S1). The results of 4-weeks old mice were consistent with the results of RNA-seq (Fig. 4). While only several genes remained elevated in 12-weeks old OI mice (*Tnf*α, *Lif*, and *Ccl2*) (Fig. S1), which might be related to the relieved bone phenotype in adulthood. IL-17A and TNFα have been proved to play an essential role in inflammatory bone erosion by inducing the production of RANKL (*Weitzmann, 2017*; *Zhao et al., 2012*). IL-17A can also promote TNFα secretion. *Matthews et al. (2017)* found the increased serum level of Tnf in homozygous oim mice, however, anti-TNFα therapy failed to reduce bone absorption. These results suggested that blocking Tnf signaling alone is insufficient to effectively reverse the excessive bone resorption in OI bones. Targeting both IL-17 and Tnf signalings may be an efficient strategy for OI treatment.

CONCLUSIONS

This study preliminarily revealed the dysregulated biological process of cellular response to Ifn together with upregulated IL-17 signaling, Tnf signaling and osteoclast differentiation in young male OI BM niche by RNA-seq. Either defective collagen production or abnormal collagen assembly shared similar alterations in gene profiles and pathways involving inflammation and osteoclast activation. Data presented here not only contributed to understanding the mechanism of the enhanced bone absorption in the bone of OI, but also provided more evidence to develop potential anti-inflammation therapies.

ADDITIONAL INFORMATION AND DECLARATIONS

Funding

The present study was supported by grants from the National Key R & D Program of China (2017YFC1001904). The funders had no role in study design, data collection and analysis, decision to publish, or preparation of the manuscript.

Grant Disclosures

The following grant information was disclosed by the authors:
National Key R & D Program of China: 2017YFC1001904.

Competing Interests

The authors declare that they have no competing interests.

Author Contributions

- Chenyi Shao conceived and designed the experiments, performed the experiments, analyzed the data, prepared figures and/or tables, authored or reviewed drafts of the article, and approved the final draft.
- Yi Liu conceived and designed the experiments, analyzed the data, prepared figures and/or tables, authored or reviewed drafts of the article, and approved the final draft.
- Jiaci Li conceived and designed the experiments, performed the experiments, prepared figures and/or tables, authored or reviewed drafts of the article, and approved the final draft.
- Ziyun Liu performed the experiments, prepared figures and/or tables, authored or reviewed drafts of the article, and approved the final draft.
- Yuxia Zhao analyzed the data, authored or reviewed drafts of the article, and approved the final draft.
- Yaqing Jing analyzed the data, authored or reviewed drafts of the article, and approved the final draft.
- Zhe Lv analyzed the data, authored or reviewed drafts of the article, and approved the final draft.
- Ting Fu analyzed the data, authored or reviewed drafts of the article, and approved the final draft.
- Zihan Wang analyzed the data, authored or reviewed drafts of the article, and approved the final draft.
- Guang Li analyzed the data, authored or reviewed drafts of the article, and approved the final draft.

Animal Ethics

The following information was supplied relating to ethical approvals (*i.e.*, approving body and any reference numbers):

The study was approved by the Animal Care and Use Committee of Tianjin Medical University (TMUaMEC 2017012).

Ethics

The following information was supplied relating to ethical approvals (*i.e.*, approving body and any reference numbers):

The study was approved by The Animal Ethical and Welfare Committee (AEWC) (TMUaMEC 2017012).

Data Availability

The following information was supplied regarding data availability:

The RNA-seq data is available at NCBI SRA: PRJNA835622.

Supplemental Information

Supplemental information for this article can be found online at http://dx.doi.org/10.7717/peerj.13963#supplemental-information.

REFERENCES

Berg S. 2021. Pediatric bone marrow alterations. *Radiologe* **61(1)**:87–108 DOI 10.1007/s00117-020-00792-1.

Biros E, Malabu UH, Vangaveti VN, Birosova E, Moran CS. 2022. The IFN-gamma/miniTrpRS signaling axis: an insight into the pathophysiology of osteoporosis and therapeutic potential. *Cytokine & Growth Factor Reviews* **64(8)**:7–11 DOI 10.1016/j.cytogfr.2022.01.005.

Boyle WJ, Simonet WS, Lacey DL. 2003. Osteoclast differentiation and activation. *Nature* **423(6937)**:337–342 DOI 10.1038/nature01658.

Brunetti G, Papadia F, Tummolo A, Fischetto R, Nicastro F, Piacente L, Ventura A, Mori G, Oranger A, Gigante I, Colucci S, Ciccarelli M, Grano M, Cavallo L, Delvecchio M, Faienza MF. 2016. Impaired bone remodeling in children with osteogenesis imperfecta treated and untreated with bisphosphonates: the role of DKK1, RANKL, and TNF-alpha. *Osteoporosis International* **27(7)**:2355–2365 DOI 10.1007/s00198-016-3501-2.

Chipman SD, Sweet HO, McBride DJ Jr, Davisson MT, Marks SC Jr., Shuldiner AR, Wenstrup RJ, Rowe DW, Shapiro JR. 1993. Defective pro alpha 2(I) collagen synthesis in a recessive mutation in mice: a model of human osteogenesis imperfecta. *Proceedings of the National Academy of Sciences* **90(5)**:1701–1705 DOI 10.1073/pnas.90.5.1701.

Ciucci T, Ibanez L, Boucoiran A, Birgy-Barelli E, Pene J, Abou-Ezzi G, Arab N, Rouleau M, Hebuterne X, Yssel H, Blin-Wakkach C, Wakkach A. 2015. Bone marrow Th17 TNFalpha cells induce osteoclast differentiation, and link bone destruction to IBD. *Gut* **64(7)**:1072–1081 DOI 10.1136/gutjnl-2014-306947.

Feng W, Guo J, Li M. 2019. RANKL-independent modulation of osteoclastogenesis. *Journal of Oral Biosciences* **61(1)**:16–21 DOI 10.1016/j.job.2019.01.001.

Forlino A, Cabral WA, Barnes AM, Marini JC. 2011. New perspectives on osteogenesis imperfecta. *Nature Reviews Endocrinology* **7(9)**:540–557 DOI 10.1038/nrendo.2011.81.

Grafe I, Yang T, Alexander S, Homan EP, Lietman C, Jiang MM, Bertin T, Munivez E, Chen Y, Dawson B, Ishikawa Y, Weis MA, Sampath TK, Ambrose C, Eyre D, Bachinger HP, Lee B. 2014. Excessive transforming growth factor-beta signaling is a common mechanism in osteogenesis imperfecta. *Nature Medicine* **20(6)**:670–675 DOI 10.1038/nm.3544.

Herrmann M, Jakob F. 2019. Bone marrow niches for skeletal progenitor cells and their inhabitants in health and disease. *Current Stem Cell Research & Therapy* **14(4)**:305–319 DOI 10.2174/1574888X14666190123161447.

Hoyer-Kuhn H, Netzer C, Semler O. 2015. Osteogenesis imperfecta: pathophysiology and treatment. *Wiener Medizinische Wochenschrift* **165(13–14)**:278–284 DOI 10.1007/s10354-015-0361-x.

Iwamoto J, Takeda T, Ichimura S. 2002. Increased bone resorption with decreased activity and increased recruitment of osteoblasts in osteogenesis imperfecta type I. *Journal of Bone and Mineral Metabolism* **20(3)**:174–179 DOI 10.1007/s007740200025.

Liu Y, Ju M, Wang Z, Li J, Shao C, Fu T, Jing Y, Zhao Y, Lv Z, Li G. 2020. The synergistic effect of NELL1 and adipose-derived stem cells on promoting bone formation in osteogenesis imperfecta treatment. *Biomedicine & Pharmacotherapy* **128(1)**:110235 DOI 10.1016/j.biopha.2020.110235.

Liu Y, Wang JH, Liu S, Kuang MJ, Jing YQ, Zhao YX, Wang ZH, Li G. 2019. A novel transgenic murine model with persistently brittle bones simulating osteogenesis imperfecta type I. *Bone* **127(10028)**:646–655 DOI 10.1016/j.bone.2019.07.021.

Lopez Franco GE, Huang A, Pleshko Camacho N, Blank RD. 2005. Dental phenotype of the col1a2(oim) mutation: DI is present in both homozygotes and heterozygotes. *Bone* **36(6)**:1039–1046 DOI 10.1016/j.bone.2005.03.004.

Marom R, Rabenhorst BM, Morello R. 2020. Osteogenesis imperfecta: an update on clinical features and therapies. *European Journal of Endocrinology* **183(4)**:R95–R106 DOI 10.1530/EJE-20-0299.

Matthews BG, Roeder E, Wang X, Aguila HL, Lee SK, Grcevic D, Kalajzic I. 2017. Splenomegaly, myeloid lineage expansion and increased osteoclastogenesis in osteogenesis imperfecta murine. *Bone* **103**:1–11 DOI 10.1016/j.bone.2017.06.004.

McBride DJ Jr., Shapiro JR, Dunn MG. 1998. Bone geometry and strength measurements in aging mice with the oim mutation. *Calcified Tissue International* **62(2)**:172–176 DOI 10.1007/s002239900412.

Michalska A, Blaszczyk K, Wesoly J, Bluyssen HAR. 2018. A positive feedback amplifier circuit that regulates interferon (IFN)-stimulated gene expression and controls Type I and Type II IFN responses. *Frontiers in Immunology* **9**:551 DOI 10.3389/fimmu.2018.01135.

Nijhuis WH, Eastwood DM, Allgrove J, Hvid I, Weinans HH, Bank RA, Sakkers RJ. 2019. Current concepts in osteogenesis imperfecta: bone structure, biomechanics and medical management. *Journal of Children's Orthopaedics* **13(1)**:1–11 DOI 10.1302/1863-2548.13.180190.

Ono T, Nakashima T. 2018. Recent advances in osteoclast biology. *Histochemistry and Cell Biology* **149(4)**:325–341 DOI 10.1007/s00418-018-1636-2.

Paterson CR, McAllion S, Stellman JL. 1984. Osteogenesis imperfecta after the menopause. *New England Journal of Medicine* **310(26)**:1694–1696 DOI 10.1056/NEJM198406283102602.

Saban J, Zussman MA, Havey R, Patwardhan AG, Schneider GB, King D. 1996. Heterozygous oim mice exhibit a mild form of osteogenesis imperfecta. *Bone* **19(6)**:575–579.

Saito M, Marumo K. 2015. Effects of collagen crosslinking on bone material properties in health and disease. *Calcified Tissue International* **97(3)**:242–261 DOI 10.1007/s00223-015-9985-5.

Takayanagi H, Sato K, Takaoka A, Taniguchi T. 2005. Interplay between interferon and other cytokine systems in bone metabolism. *Immunological Reviews* **208(1)**:181–193 DOI 10.1111/j.0105-2896.2005.00337.x.

Takeyari S, Kubota T, Ohata Y, Fujiwara M, Kitaoka T, Taga Y, Mizuno K, Ozono K. 2021. 4-Phenylbutyric acid enhances the mineralization of osteogenesis imperfecta iPSC-derived osteoblasts. *Journal of Biological Chemistry* **296**:100027 DOI 10.1074/jbc.RA120.014709.

Tilg H, Moschen AR, Kaser A, Pines A, Dotan I. 2008. Gut, inflammation and osteoporosis: basic and clinical concepts. *Gut* **57(5)**:684–694 DOI 10.1136/gut.2006.117382.

Tsukasaki M, Takayanagi H. 2019. Osteoimmunology: evolving concepts in bone-immune interactions in health and disease. *Nature Reviews Immunology* **19(10)**:626–642 DOI 10.1038/s41577-019-0178-8.

Weitzmann MN. 2017. Bone and the immune system. *Toxicologic Pathology* **45(7)**:911–924 DOI 10.1177/0192623317735316.

Weyand CM, Goronzy JJ. 2021. The immunology of rheumatoid arthritis. *Nature Immunology* **22(1)**:10–18 DOI 10.1038/s41590-020-00816-x.

Yao WL, Wen Q, Zhao HY, Tang SQ, Zhang YY, Wang Y, Xu LP, Zhang XH, Huang XJ, Kong Y. 2021. Different subsets of haematopoietic cells and immune cells in bone marrow between young and older donors. *Clinical and Experimental Immunology* **203(1)**:137–149 DOI 10.1111/cei.13531.

Zhao B, Grimes SN, Li S, Hu X, Ivashkiv LB. 2012. TNF-induced osteoclastogenesis and inflammatory bone resorption are inhibited by transcription factor RBP-J. *Journal of Experimental Medicine* **209(2)**:319–334 DOI 10.1084/jem.20111566.

Zhytnik L, Maasalu K, Reimann E, Martson A, Koks S. 2020. RNA sequencing analysis reveals increased expression of interferon signaling genes and dysregulation of bone metabolism affecting pathways in the whole blood of patients with osteogenesis imperfecta. *BMC Medical Genomics* **13(1)**:177 DOI 10.1186/s12920-020-00825-7.